

Electrochemical and Surface Characterization of a New Ti-Ta-Zr Alloy Covered with Biomimetic Bovine Serum Albumin

C. Vasilescu, S. I. Drob*, M. Popa, J. M. Calderon Moreno, M. Anastasescu, M. Marcu

Institute of Physical Chemistry “Ilie Murgulescu” of Romanian Academy, Spl. Independentei 202,
060021, Bucharest, Romania

*E-mail: sidrob.icf@gmail.com

Received: 6 May 2016 / Accepted: 4 June 2016 / Published: 7 July 2016

The surface of the new ternary Ti-15Ta-5Zr alloy was functionalized with bovine serum albumin (BSA) deposited by chemical method adapted to the composition of the alloy and its passive film. The BSA deposition was proved by atomic force microscopy (AFM), scanning electron microscopy (SEM) and Raman micro-spectroscopy techniques; also, its electrochemical behavior and corrosion resistance in physiological Ringer solution of different pH values (simulating the real functional conditions of an implant) were performed by cyclic potentiodynamic and linear polarization and electrochemical impedance spectroscopy (EIS). The BSA coating consists from cvasispherical aggregates (AFM) with high roughness which can promote the osteoblast cell development. SEM micrographs revealed a thick deposition with some porosity. EDX spectrum identified C and N elements from BSA and Ca and P from the deposition solution (Ringer) which can stimulate the bone formation. Raman spectra showed the similar composition of BSA powder and BSA deposited on the Ti-15Ta-5Zr alloy surface. Electrochemical parameters have more favorable values for the BSA coated alloy comparing with the bare alloy proving nobler electrochemical behavior, better passive ability of the BSA coated alloy. Corrosion parameters have superior values of about 3-10 times than those of the bare alloy, namely, the BSA coating is both protective and slightly porous permitting the interactions with the human biofluid. The impedance results were fitted with two time constants electric equivalent circuit for the bare alloy and with three time constants for the coated alloy.

Keywords: Biomimetic surface fuctionalization, AFM, SEM, EIS, Cyclic potentiodynamic and linear polarization

1. INTRODUCTION

Metallic implant materials are generally biochemical inert and do not stimulate the bone cell adhesion and development. Also, the metallic surfaces covered with the bioactive hydroxyapatite are

osteoconductive but have a reduced osteoinductive activity [1]. For this reason was necessary to develop application methods of osteogenic factors on their surfaces. Bruder et al. [2] used proteins as fibrinogen, fibronectin, vitronectin which quickly absorb on the surface and constitute good matrix for the adhesion and proliferation of the stem mesenchymal cells which displace to the area of suffering bone and generate a new matrix where the osteoblast cells adhere and differentiate forming new health bone [3]. Ananthanarayanan et al. [4] prepared synthetic peptides amphiphiles which synergistically acted for the development and proliferation of the stem cells and then for the regeneration of bone cells. LeBaron et al. [5] applied peptides by a laborious procedure that did not give good results. Other peptides were used to prevent the implant infections by their antimicrobial properties [6]. Hu et al. [7] functionalized the titanium surface with dopamine, carboxymethyl chitosan, hyaluronic acid-catechol or polysaccharides and improved both the osteoblast functions and antibacterial activity of the substrate. Huang et al. [8] obtained a biomimetic, bi-layered platform using multi-component proteins (collagen and/or fibronectin) conjugated with lipids that stimulated the adhesion and spreading of fibroblast cells. Oliva et al. [9] deposited human serum albumin on the oxidized titanium surface and the electrochemical studies showed that this protein decreased the corrosion rate of the metallic support by the blocking of the electrochemical active areas. Uchida et al. [10] realized a biomimetic composite of laminin-apatite coating with very good cell-adhesion properties. The human serum albumin deposited on Ti surface [11] as a molecular layer increased the protein spreading. In the some time, the adsorption of the bovine serum albumin onto stainless steel surface [12] was proved by AFM, protein radiolabeling and quartz crystal microbalance. Other authors [13] fabricated a novel composite scaffold bioglass-collagen-phosphatidylserine that enhanced the bone formation.

From above presentation resulted that the incipient studies existing till now have applications dedicated to specifically materials. In this paper we functionalized the surface of the new ternary Ti-15Ta-5Zr alloy with bovine serum albumin (BSA) deposited by chemical method adapted to the composition of the alloy and its passive film. The BSA deposition was proved by atomic force microscopy (AFM), scanning electron microscopy (SEM) and Raman micro-spectroscopy techniques; also, its electrochemical behavior and corrosion resistance in physiological Ringer solution of different pH values (simulating the real functional conditions of an implant) were performed by cyclic potentiodynamic and linear polarization and electrochemical impedance spectroscopy (EIS).

2. EXPERIMENTAL PART

2.1. Deposition of BSA coating

Discs obtained from Ti-15Ta-5Zr casting ingots were cut at a diameter of 1 cm. and thickness of 1 mm. The samples were ground with metallographic paper till 600 grades to assure a proper roughness for the subsequent deposition of BSA.

The deposition solution (Ringer solution of pH = 7.4) contained 2 g/L bovine serum albumin. Ringer solution had the following composition (g/L): NaCl – 6.8; KCl – 0.4; CaCl₂ – 0.2; MgSO₄·7H₂O – 0.2048; NaH₂PO₄·H₂O – 0.1438; NaHCO₃ -1.1; glucose – 1. The samples were

immersed in the deposition solution at temperature of 37⁰C (controlled by a digital oven) for 144 hours. Then, the samples were washed with Millipore water and dried in air.

2.2. Surface characterization of BSA coating

The topography and roughness of the BSA coating were examined by atomic force microscope type XE-100 that supplied 2D and 3D topographical images and line profile obtained in non-contact mode on 2 x 2 μm area. The root mean square roughness (RMS) and average surface roughness (Rav) were determined by statistical analysis of the equipment own program.

The microstructure and morphology of the BSA coating were studied by scanning electron microscope type FEI Quanta 3D FEG working at accelerated voltage of 20 kV, equipped with energy-dispersive X-ray (EDX) detector for the elemental analysis.

The composition of the deposited BSA coating was investigated in comparison with BSA powder. The Raman micro-spectroscope type LABRam Jobin Yvon used the green line ($\lambda = 514.5$ nm) of Ar⁺ laser (spot of $\approx 1 - 2$ μm) at a power of ≈ 20 mW and acquisition time of 40 s. Raman spectra (RS) covered a range of 0 cm⁻¹ till 4000 cm⁻¹ and a 90x microscope objective was used.

2.3. Electrochemical characterization of BSA coating

The electrochemical BEHAVIOR of the BSA coating was determined using the cyclic potentiodynamic and linear polarization and electrochemical impedance spectroscopy (EIS) methods in Ringer solution of the same composition from Chapter 2.1.) of neutral (7.4) and alkaline (8.98) pH values which simulate the real functional conditions of an implant; the normal pH of the human biofluid is about 7.4, but in the case of infections or inflammations, the pH value can increase till 9 value [14].

The cyclic potentiodynamic polarization was applied from -800 mV (vs. SCE) till +1000 mV (vs. SCE) with the aim to cover the whole potential domain that can exist in the human body [15-17]. The voltammograms were conducted with a scan rate of 1 mV/s by Voltalab 80 equipment with its VoltaMaster program. From cyclic potentiodynamic curves were quantified the main electrochemical parameters [18]: corrosion potential, E_{corr} as zero current potential; passivation potential, E_p of the constant current; tendency to passivation as $|E_{\text{corr}} - E_p|$ difference (low values show a very easy, rapid passivation); passive current density, i_p as the average value from the passive potential domain.

The linear polarization was performed with the same Voltalab 80 equipment for ± 100 mV around the open circuit potential using a scan rate 0.1 mV/s. The VoltaMaster 4 program adjusted Tafel representations and directly delivered the values of: corrosion current density, i_{corr} ; corrosion rate, V_{corr} ; ion release rate; polarization resistance, R_p .

The coating porosity, P (%) was calculated [19, 20] as the ratio between the resistance R_u of the uncovered surface and the resistance R_c of the covered surface:

$$P(\%) = \frac{R_u}{R_c} \times 100 \quad (1)$$

The coating efficiency E (%) was calculated [21, 22] depending on the corrosion current density for the uncovered $i_{corr,u}$ and covered $i_{corr,c}$ alloy surface:

$$E(\%) = \frac{i_{corr,u} - i_{corr,c}}{i_{corr,u}} \tag{2}$$

Electrochemical impedance spectroscopy measurements were carried out at open circuit potential, in 10^{-1} Hz – 10^5 Hz frequency range at a sine wave of 5 mV. From Nyquist and Bode spectra were fitted the electric equivalent circuits using Zview program.

3. RESULTS AND DISCUSSION

3.1. Surface analysis of BSA coating

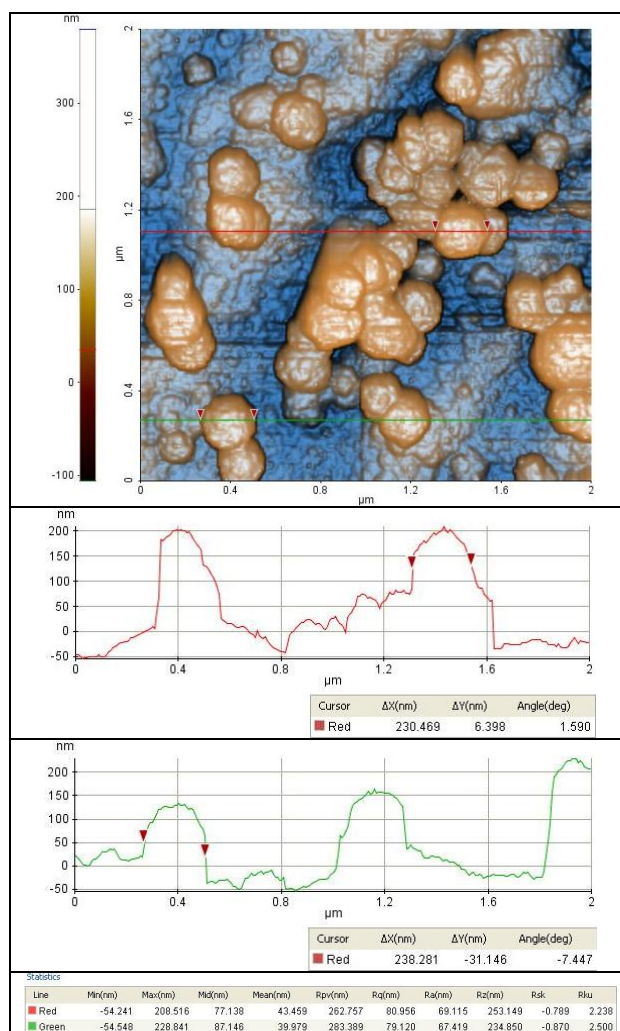


Figure 1. 3D images and line profile of BSA coating deposited on Ti-15Ta-5Zr alloy surface.

The 3D AFM images (Fig. 1) of the BSA coating show the deposition of cvasispherical aggregates with dimensions varying between 200 nm and 300 nm which represent a rough surface; the

line profile evinces high differences between maximum and minimum which can promote the adhesion and proliferation of cells [23-26]. RMS roughness has a value of 76.8 nm and R_{av} of 60.8 nm which can promote the cell development.

SEM micrographs [27, 28] (Fig. 2a) confirm the AFM results, namely, thick deposition of spherical particles with some pores. EDX spectrum (Fig. 2b) detected carbon, C and nitrogen, N elements specifically to BSA protein; in addition, calcium, Ca and phosphor, P elements, the main inorganic components of the human bone appear; these elements can stimulate the bone formation. Also, in EDX spectrum of BSA coating appear the constituent elements of the alloy (Ti, Ta, Zr) from the substrate.

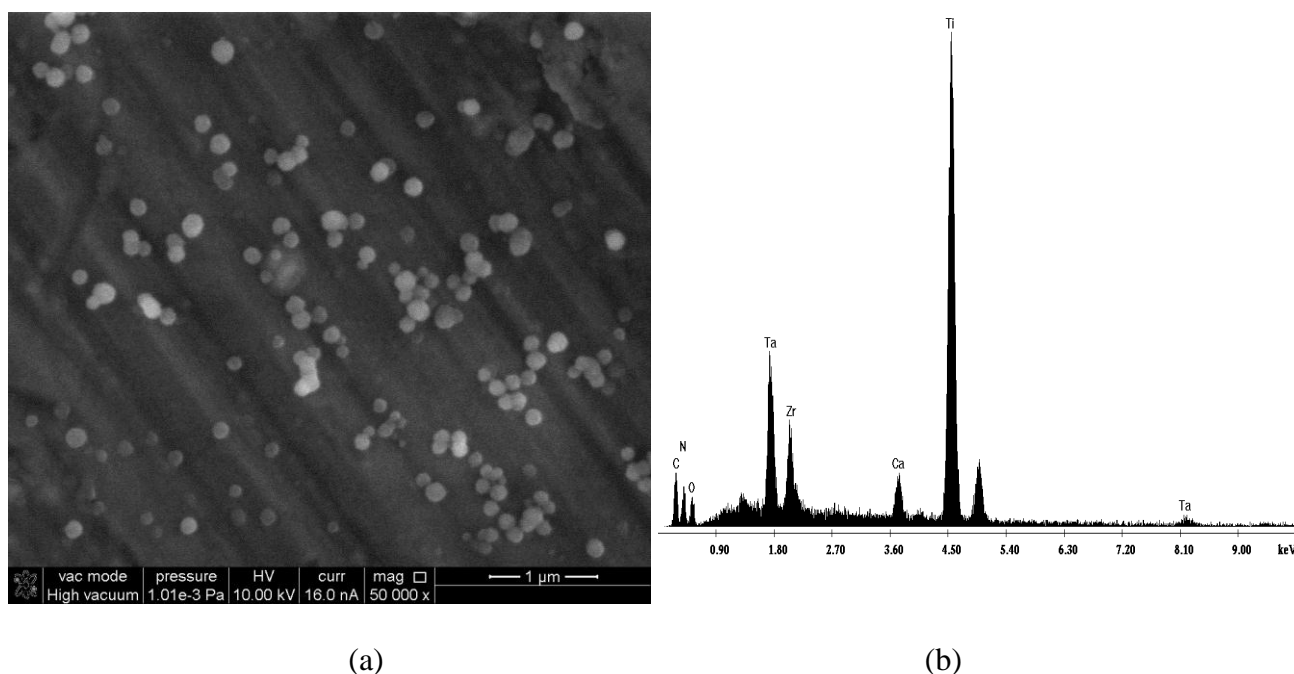


Figure 2. SEM micrographs (a) and EDX spectrum (b) of BSA coating deposited on Ti-15Ta-5Zr alloy surface.

The analysis of the Raman Spectra of proteins is complex because of the many different contributions from aromatic aminoacids, i.e. phenyl ring in phenylalanine (Phe) at ~ 620 , 1000 , 1205 , 1610 cm^{-1} , tryptophan (Trp) at ~ 750 , 1340 cm^{-1} , tyrosine (Tyr) at 640 , 830 - 850 doublet, 1175 and 1205 cm^{-1} , the polypeptide backbone secondary structure (the strong amide I band at $\sim 1655 \text{ cm}^{-1}$, and the weak amide II band at $\sim 1550 \text{ cm}^{-1}$ and amide III band at ~ 1240 - 1270 cm^{-1}), functional groups (i.e. CH at $\sim 1447 \text{ cm}^{-1}$) and environmental effects [29-32]. The scope of the Raman study was to determine if there were changes in the secondary structure of the BSA deposited on the alloy surface, comparing with the RS of BSA in the solid state. We can observe similar contributions in both measured spectra (Fig. 3). The sharp intense band measured at 1000 cm^{-1} corresponds to the aromatic aminoacid phenylalanine. This band is not sensitive to conformational changes of the protein, and can be used as an internal standard reference for the Raman spectra; therefore the observed decrease in relative intensity is not related to any structural change. The tyrosine typical doublet Raman bands at 830 and

850 cm^{-1} are observed, also the Fermi doublet of Trp (1340 and 1360 cm^{-1}) that serves as an hydrophobicity marker. The absence of any band at 1360 cm^{-1} together with the clear band at 1340 cm^{-1} indicates the lack of hydrophobic bonds (BSA is water-soluble). The amide I vibrational band, in the range 1600-1700 cm^{-1} , is commonly used for secondary structure analysis. This band remains unchanged in both shape and relative intensity in the RS of deposited BSA, compared to solid state BSA, thus indicating very similar secondary structure, without changes due to deposition from solution. There is a clearly dominant contribution from the α -helix marker at $\sim 1655 \text{ cm}^{-1}$, indicative of a predominant α helical structures. Over the whole spectra, the only one significant difference that distinguish that of deposited BSA from solid state is the growth in relative intensity of the band (at $\sim 940 \text{ cm}^{-1}$) related to the $\text{C}_\alpha\text{-C}$ bond (skeletal C-C stretching vibration for the α -helix structure) and its shift towards higher Raman shifts ($\sim 955 \text{ cm}^{-1}$). We must note that this band is not usually considered as a marker of the protein structure and therefore it is not clear to us the structural change in the deposited protein or interaction with the alloy substrate that might be associated with the observed shift.

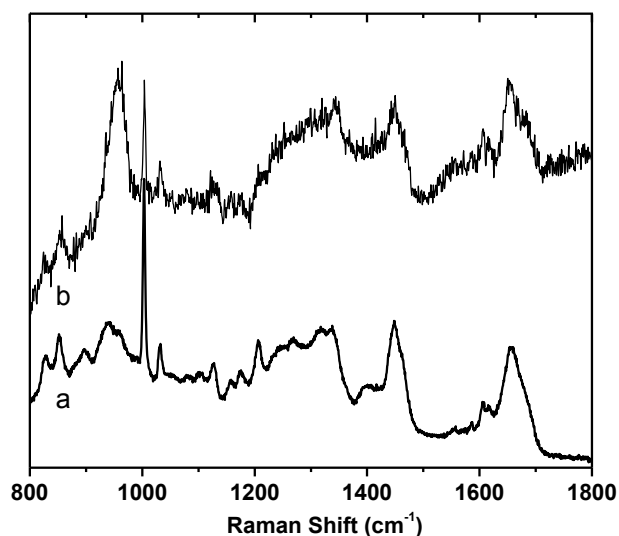


Figure 3. Raman spectra measured (a) on BSA powder and (b) on rounded deposits formed after deposition on the Ti-15Ta-5Zr alloy surface.

3.2. Electrochemical and corrosion behavior of BSA coating

3.2.1. Electrochemical behavior of BSA coating by cyclic potentiodynamic polarization method

The cyclic potentiodynamic polarization curves (Fig. 4) show passive behavior both for bare and BSA coated alloy; this behavior is characterized by a large passive potential ranges, ΔE_p ($>1000 \text{ mV}$) and a low passive current densities, i_p . For the covered alloy can be observed the ennobling of the corrosion, E_{corr} and passivation, E_p potentials and the decrease of the tendency to passivation $|E_{\text{corr}} - E_p|$ as compared with the bare alloy (Table 1).

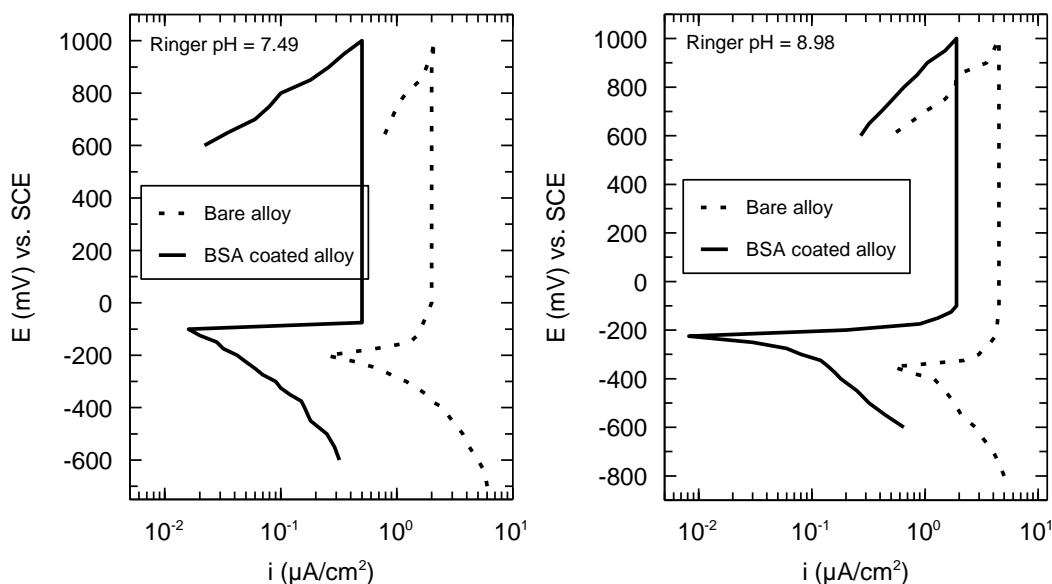


Figure 4. Cyclic potentiodynamic polarization curves for bare and BSA coated Ti-15Ta-5Zr alloy in Ringer solution at 37⁰C.

The covered alloy has a nobler electrochemical behavior than that of the bare alloy due to the protective action of the BSA coating that thickens and compactness (SEM micrographs) the native passive film, together acting as a barrier against the transfer of ions through them [9, 15, 27, 33]. The more favorable values of the electrochemical parameters prove the better passive ability of the covered alloy as result of the existence of BSA coating. Also, in neutral Ringer solution were registered the best values of the electrochemical parameters which demonstrate a better passivation in this physiological solution that represents the normal functional condition of an implant.

Table 1. Electrochemical parameters of bare and BSA covered Ti-15Ta-5Zr alloy in Ringer solution at 37⁰C.

Parameter	Ringer pH = 7.49		Ringer pH = 8.98	
	Bare	BSA covered	Bare	BSA covered
E _{corr} (mV)	-200	-100	-350	-250
E _p (mV)	-100	-75	-200	-100
ΔE _p (mV)	>1000	>1000	>1000	>1000
E _{corr} - E _p (mV)	100	25	150	150
i _p (µA/cm ²)	2.0	0.5	4.5	1.9

3.2.2. Corrosion behavior of BSA coating by linear polarization method

The linear polarization, Tafel curves (Fig. 5) and values of the corrosion parameters (Table 2) show that the corrosion current densities, i_{corr}, corrosion rates, V_{corr} and Ion release rates for the

covered alloy decreased of about 10 times as compared with the bare alloy, denoting that the coating has a better protective action. Also, the polarization resistance, R_p for the coated alloy increased of about 3 times than that of the bare alloy, namely, the BSA coating is a barrier against the crossing of ions through it [27, 34, 35]. The BSA coating has an efficiency of 80% and a porosity of 42%, i. e., the coating is both protective and slightly porous, permitting the interactions with the human biofluid.

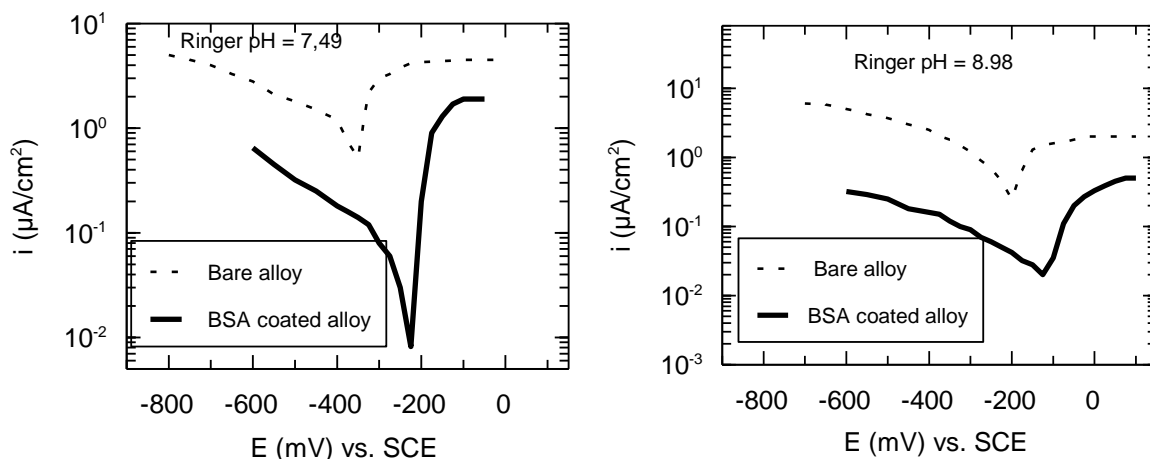


Figure 5. Tafel curves for bare and BSA coated Ti-15Ta-5Zr alloy in Ringer solution at 37⁰C.

Table 2 Corrosion parameters of bare and BSA covered Ti-15Ta-5Zr alloy in Ringer solution at 37⁰C.

Parameter	Ringer pH = 7.49		Ringer pH = 8.98	
	Bare	BSA covered	Bare	BSA covered
i_{corr} ($\mu\text{A}/\text{cm}^2$)	0.01	0.0018	0.061	0.0099
V_{corr} ($\mu\text{A}/\text{cm}^2$)	0.092	0.016	0.556	0.09
R_p ($\text{k}\cdot\Omega \text{ cm}^2$)	180	425	133	315
Ion release (ng/cm^2)	9.35	1.63	56.49	9.14
Porosity (%)	-	42.35	-	42.22
Efficiency (%)	-	82	-	83.7
Resistance class	PS	PS	PS	PS

PS – Perfect Stable

3.2.3. Behavior of BSA coating by EIS

The Nyquist spectra (Fig. 6) display semicircles with big diameters, indicating a passive film [22, 36]. The curvature radii are higher for the BSA covered alloy as result of the supplementary protection action exercised by the BSA coating. The inflexions from these spectra suggest the existence of more layers on the Ti-15Ta-5Zr alloy surface.

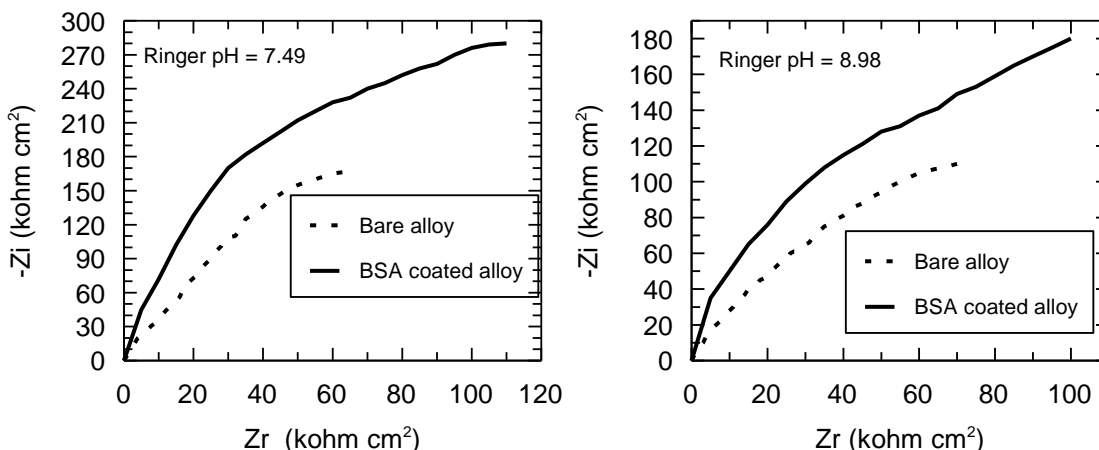


Figure 6. Nyquist spectra for bare and BSA coated Ti-15Ta-5Zr alloy in Ringer solution at 37⁰C.

Bode spectra (Fig. 7) in form of phase angle function of frequency reveal two phase angles for the bare alloy and three phase angles for the BSA coated alloy. For the bare alloy, the highest phase angle, in the low frequency range characterizes the interior interface between substrate (alloy) and the passive film; the lower phase angle from the medium frequency range describes the exterior interface between the passive film and BSA coating. The phase angle from the high frequency range represents the BSA layer [27, 28, 36]. For the BSA coated alloy, the phase angles from the low frequency range have values of $-86^{\circ} \div -84^{\circ}$ and the phase angles from the medium frequency range of $-82^{\circ} \div -80^{\circ}$, namely, a very resistant, insulating passive film in the neutral respectively alkaline Ringer solution. These values are higher than those of the bare alloy of $-84^{\circ} \div -80^{\circ}$ and $-78^{\circ} \div -76^{\circ}$, which signify a slightly lower capacitive of the bare alloy [27, 28, 22]. The third phase angle (that appears only in the case of the BSA covered alloy) from the high frequency range has values of about -45° in neutral Ringer solution and of -40° in alkaline Ringer solution; these values demonstrate the existence of a layer with some porosities where can take place some processes of adhesion and proliferation of the bone cells on the external surface [22].

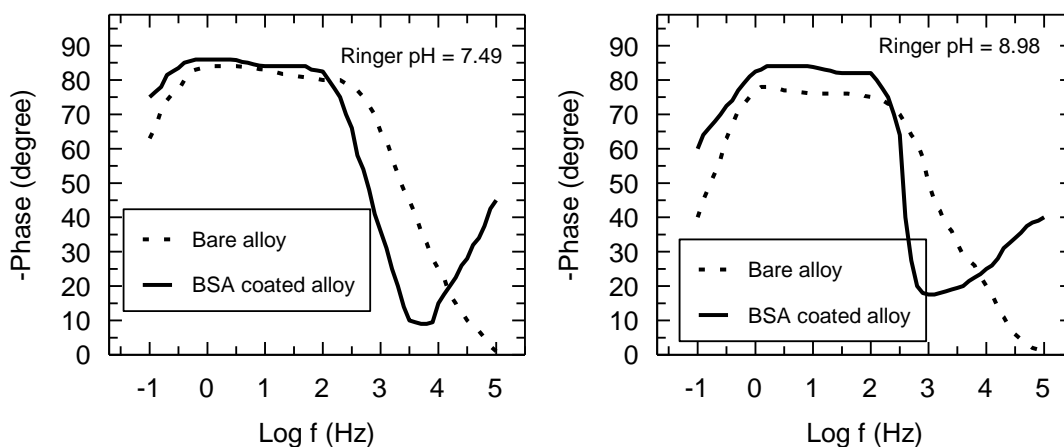


Figure 7. Bode spectra for bare and BSA coated Ti-15Ta-5Zr alloy in Ringer solution at 37⁰C.

It is known that the processes in the passive film are relaxed at low and intermediate frequency range and the processes into coating are relaxed at high frequency range [22, 36]; this fact is also confirmed by our results.

The impedance spectra for the bare alloy were modelled with an electric equivalent circuit with two time constants (Fig. 8a): the first time constant corresponds with the highest phase angle and represents the inner, insulating, barrier layer of the native passive film, illustrated by R_1 resistance and CPE_1 capacitance; the second time constant characterizes the lower phase angle and indicates a less resistant layer, identified by R_2 and CPE_2 capacitance. For the BSA covered alloy, the electric equivalent circuit was modelled (Fig. 8b) with three time constants [27, 28]: the first time constant for the inner, barrier layer of the native passive film described by R_1 resistance and CPE_1 capacitance; the second time constant for the slowly porous layer placed at the limit between passive film and BSA coating, represented by R_2 resistance and CPE_2 capacitance; the third time constant shows the BSA layer with some porosities, illustrated by R_3 resistance and CPE_3 capacitance.

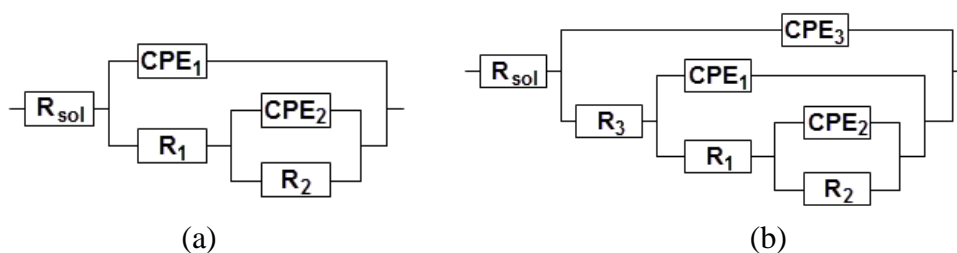


Figure 8. Electrical equivalent circuit modelled for bare (a) and BSA coated (b) Ti-15Ta-5Zr alloy in Ringer solution at 37°C.

The electrical parameters of the electric equivalent circuits (Table 3) evince the following facts:

- the value of the compact layer resistances, R_1 are 100 times higher than those of R_2 and R_3 resistances, indicating that this layer is very resistant and acts as a barrier against the corrosion [37];
- the values of R_1 and R_2 resistances are similar both bare and BSA covered alloy, that means that the BSA layer does not interact with the passive film and does not modify it [28];
- the resistances R_3 of the BSA layer have the lowest values, which denote a layer with some porosities [36]; this fact is confirmed by the SEM micrographs;
- the values of CPE_3 capacities of the BSA layer are 10 times higher than those of the compact layer CPE_1 , proving that the BSA exterior layer has some pores and has a bigger area than that of compact passive layer [22, 36];
- the values of n_1 and n_2 parameters are closed of 1 value (ideal capacitor) indicating that both the inner barrier layer and the intermediate layer (both forming the passive film) are very insulating [22];
- for the BSA coating, the lower values of n_3 parameter proves that this coating has some pores and permits that the species from the human biofluid to interact with this coating, namely this BSA layer is bioactive [22].

The impedance results evinced the dual character of the surface of the BSA covered alloy: corrosion resistance due to the compact inner layer and bioactivity due to the exterior, slowly porous BSA layer that stimulates the growth of the bone cells, favoring the alloy osteointegration.

Table 3. Electrical parameters of the equivalent circuit modelled for bare and BSA covered Ti-15Ta-5Zr alloy in Ringer solution at 37°C.

Parameter	Ringer pH = 7.49		Ringer pH = 8.98	
	Bare	BSA covered	Bare	BSA covered
R_{sol} (Ω cm ²)	14.1	14.6	13.4	13.9
R_1 (Ω cm ²)	8.7×10^6	9.1×10^6	7.5×10^6	7.8×10^6
CPE_1 (S s/cm ²)	3.1×10^{-6}	2.9×10^{-6}	2.4×10^{-6}	2.2×10^{-6}
n1	0.98	0.98	0.96	0.96
R_2 (Ω cm ²)	2.1×10^4	2.3×10^4	1.8×10^4	2.0×10^4
CPE_2 (S s/cm ²)	1.1×10^{-5}	1.0×10^{-5}	1.4×10^{-5}	1.2×10^{-5}
n2	0.92	0.89	0.91	0.90
R_3 (Ω cm ²)	-	1.2×10^4	-	1.1×10^4
CPE_3 (S s/cm ²)	-	2.6×10^{-5}	-	2.4×10^{-5}
n3	-	0.80	-	0.79

4. CONCLUSIONS

The AFM images of the BSA coating show the deposition of cvasispherical aggregates with dimensions varying between 200 nm and 300 nm which represent a rough surface; which can promote the adhesion and proliferation of cells. SEM micrographs show a thick deposition of spherical particles with some pores. EDX spectrum detected carbon, C and nitrogen, N elements specifically to BSA protein; in addition, calcium, Ca and phosphor, P elements; these elements can stimulate the bone formation. Raman spectra determined similar composition of structure of the BSA deposited on the alloy surface, comparing with the RS of BSA in the solid state.

The covered alloy has a nobler electrochemical behavior than that of the bare alloy due to the protective action of the BSA coating that thickens and compactness (SEM micrographs) the native passive film, together acting as a barrier against the transfer of ions through them.

Values of the corrosion parameters show that the corrosion current densities, corrosion rates, and Ion release rates for the covered alloy decreased of about 10 times and polarization resistance increased of about 3 times as compared with the bare alloy, denoting that the coating has a better protective action. The impedance spectra for the bare alloy were modelled with an electric equivalent circuit with two time constants and for the BSA coated alloy with three time constants. The impedance

results evinced the dual character of the surface of the BSA covered alloy: corrosion resistance and bioactivity that stimulates the growth of the bone cells, favoring the alloy osteointegration.

References

1. B.K. Culpepper, M.C. Phipps, P.B. Bonvallet, S.L. Bellis, *Biomaterials* 31 (2010) 9586
2. S.P. Bruder, N. Jaiswal, N.S. Ricalton, J.D. Mosca, K.H. Kraus, S. Kadiyala, *Clin. Orthop. Relat. Res.* 284 (1998) S247
3. K.M. Hennessy, B.E. Pollot, W.C. Clem, M.C. Phipps, A.A. Sawyer, B.K. Culpepper, S.L. Bellis, *Biomaterials* 30 (2009) 1898
4. B. Ananthanarayanan, L. Little, D.V. Schaffer, K.E. Healy, *Biomaterials* 31 (2010) 8706
5. R.G. LeBaron, K.A. Athanasiou, *Tissue Eng.* 6 (2000) 85
6. M. Kazemzadeh-Narbat, J. Kindrachuk, K. Duan, H. Jenssen, R.E.W. Hancock, *Biomaterials* 31 (2010) 9519
7. X. Hu, K.-G. Neoh, Z. Shi, E.-T. Kang, C. Poh, W. Wang, *Biomaterials* 31 (2010) 8854
8. C.-J. Huang, P.-Y. Tseng, Y.-C. Chang, *Biomaterials* 31 (2010) 7183
9. F.Y. Oliva, L.B. Avalle, O.R. Camara, *J. Electroanal. Chem.* 534 (2002) 19
10. M. Uchida, A. Oyane, H.-M. Kim, T. Kokubo, A. Ito, *Adv. Mater.* 16 (2004) 1071
11. I. Van De Keere, R. Willaert, E. Tourwe, A. Hubin, J. Vareecken, *Surf. Interface Anal.* 40 (2008) 157
12. M.P. Gispert, A.P. Serro, R. Colaco, B. Saramago, *Surf. Interface Anal.* 40 (2008) 1529
13. C. Hu, P. Su, X. Chen, Y. Meng, W. Yu, A.P. Xiang, Y. Wang, *Biomaterials* 32 (2011) 1051
14. R van Noort, *J. Mater. Sci.* 22 (1987) 3801
15. J. Black, *Biological performance of materials: Fundamentals of biocompatibility*, M. Decker Inc. NY, 1992.
16. A. Cigada, M. Gabrini, P. Dedeferrri, *J. Mater. Sci.: Mater. Med.* 3 (1992) 408
17. G. Rondelli, B. Vicentini, *Biomaterials* 23 (2002) 639
18. E. Vasilescu, P. Drob, D. Raducanu, I. Cinca, D. Mareci, J.M. Calderon Moreno, M. Popa, C. Vasilescu, J.C. Mirza Rosca, *Corros. Sci.* 51 (2009) 2885
19. V. Tato, D. Landolt, *J. Electrochem. Soc.* 145 (1998) 417
20. J.C. Caicedo, C. Amaya, G. Cabrera, J. Esteve, W. Aperador, M.E. Gomez, P. Prieto, *Thin Solid Films* 519 (2011) 6362
21. E.-J. Kim, Y.-H. Jeong, H.-C. Choe, W.A. Bradley, *Appl. Surf. Sci.* 258 (2012) 2083
22. D. Roman, J.C. Bernardi, C.D. Boeira, F.S. de Souza, A. Spinelli, C.A. Figueroa, R.L.O. Basso, *Surf. Coat. Technol.* 206 (2012) 4645
23. E. Alcamo, *The microbiology coloring book*, AddisonWesley, New York, 1995
24. C.P. Kurtzman, J.W. Fell, *Surf. Coat. Technol.* 233 (2013) 27
25. R.B. Heimann, *Surf. Coat. Technol.* 233 (2013) 27
26. J. Jakubowicz, G. Adamek, M.U. Jurczyk, *Mater. Charact.* 70 (2012) 55
27. R. Hang, S. Ma, V. Ji, P.K. Chu, *Electrochim. Acta* 55 (2010) 5551
28. L.T. Duarte, S.R. Biaggio, R.C. Rocha-Filho, N. Bocchi, *J. Mater. Sci.: Mater. Med.* 22 (2011) 1663
29. J.P. Biscar, P. Dhall, J. Pennison, *Chem. Phys. Letters*, 14 (1972) 569
30. B. A. Bolton, J. R. Scherer, *J. Phys. Chem.* 22 (1989) 7635
31. C. David, S. Foley, C. Mavon, M. Enescu, *Biopolymers* 89 (2008) 623
32. R. Lu, W.-W. Li, A. Katzir, Y. Raichlin, H.-Q. Yu, B. Mizaikoff, *Analys* 140 (2015) 765
33. D.J. Blackwood, A.W.C. Chua, K.H.W. Seah, R. Thampuran, *Corros. Sci.* 42 (2000) 481

34. A.K. Shukla, R. Balasuprabramiam, *Corros. Sci.* 48 (2006) 1696
35. A.W.E. Hodgson, Y. Mueller, D. Forster, S. Virtanen, *Electrochim. Acta* 47 (2002) 1913
36. C.X. Wang, *Biomaterials* 24 (2003) 3069
37. A. Balamurugan, G. Balossier, S. Kannan, J. Michel, J. Faure, S. Rajeswari, *Ceram. Int.* 33 (2007) 605

© 2016 The Authors. Published by ESG (www.electrochemsci.org). This article is an open access article distributed under the terms and conditions of the Creative Commons Attribution license (<http://creativecommons.org/licenses/by/4.0/>).